Journal of Materials Chemistry

Cite this: J. Mater. Chem., 2012, 22, 8793

www.rsc.org/materials

PAPER

Near UV-pumped yellow-emitting Eu^{2+}-doped $Na_3K(Si_{1-x}Al_x)_8O_{16\pm\delta}$ phosphor for white-emitting LEDs

Ji Yeon Han,[a] Won Bin Im,[b] Ga-yeon Lee[a] and Duk Young Jeon*[a]

Received 21st December 2011, Accepted 12th February 2012
DOI: 10.1039/c2jm16739e

A novel yellow-emitting phosphor, $Na_3K(Si_{1-x}Al_x)_8O_{16\pm\delta}:Eu^{2+}$, peaking at 555 nm was synthesized and evaluated as a candidate for white-emitting LEDs. The structure refinement, luminescence properties of $Na_3K(Si_{1-x}Al_x)_8O_{16\pm\delta}:Eu^{2+}$ phosphors as well as their thermal quenching and the fabrication of white-emitting LEDs were for the first time investigated. By partially substituting Si^{4+} with Al^{3+}, the emission peak was shifted from 553 nm to 573 nm, giving a greenish yellow–yellow color, due to the splitting of the 5*d* energy level of Eu^{2+}. By using a near-UV LED (395 nm) and a mixture of yellow-emitting $Na_3K(Si_{1-x}Al_x)_8O_{16\pm\delta}:Eu^{2+}$ phosphor and blue-emitting $BaMgAl_{10}O_{17}:Eu^{2+}$ phosphor as light converters, we constructed an intense white-light-emitting LED. The white-light-emitting LED exhibited an excellent color-rendering index R_a of 90 at a correlated color temperature of 5952 K with CIE coordinates of (0.33, 0.29). The results of the white-emitting LED package combining 395 nm near UV chip with Y/B phosphors demonstrated the potential of the yellow-emitting $Na_3K(Si_{1-x}Al_x)_8O_{16\pm\delta}:Eu^{2+}$ phosphor for UV LED application.

1 Introduction

Recently, the field of solid-state lighting based on GaN semiconductors has seen remarkable breakthroughs in efficiency.[1] Essentially, it is expected that white-light-emitting diodes (LEDs) can offer advantages of significant power saving, long lifetime, high luminous efficiency, and environmental friendliness.[2,3] The conventional way involves combining a blue-emitting LED with a yellow-emitting $Y_3Al_5O_{12}:Ce^{3+}$ (YAG:Ce^{3+}) phosphor which is relatively easy to fabricate and commercialized.[4,5] Although a blue-emitting LED chip with the yellow-emitting YAG:Ce^{3+} phosphor has high efficiency (>100 lm W^{-1}), the white LED based on the YAG:Ce^{3+} phosphor exhibits a poor color rendering index (CRI ≈ 70 to 80) and a high correlated color temperature (CCT ≈ 7750 K)[6] because it lacks a red component which is not suitable for applications requiring high CRI properties, such as residential and medical lighting.[7–9]

In recent years, white-emitting LEDs fabricated using near-ultraviolet (n-UV) LED or ultraviolet LED with three primary color emissions mixed from three individual phosphors have been investigated to improve the CRI and to tune the CCT.[10] However, the white-emitting LEDs which adopt UV-pumped R, G, and B phosphors have problems with the low efficiency of the phosphor that converts UV light into red, green and blue colors. White LEDs fabricated using an n-UV LED coupled with a blend of yellow-and blue-emitting phosphors have exhibited favorable properties, including tunable CCTs, tunable Commission International de I'Eclairage (CIE) chromaticity coordinates, and excellent CRI values.[11] Therefore, it is important to develop new yellow-emitting phosphors for n-UV LED applications. Eu^{2+}-doped phosphor generally shows superior absorption in the spectral region of 250–400 nm, and because the 4*f*–5*d* transition of the Eu^{2+} ion is sensitive to the crystal field and covalency, the Eu^{2+}-doped silicate has strong absorption in the UV-to-visible spectral region and exhibits broad emission bands from blue to red.[12,13] Many yellow-emitting phosphors with Eu^{2+} activated for n-UV LEDs have been reported, including $Sr_3B_2O_6:Eu^{2+}$,[14] $Ca_2BO_3Cl:Eu^{2+}$,[15] $Li_2SrSiO_4:Eu^{2+}$,[16] $Sr_2SiO_4:Eu^{2+}$,[17] $Ca_3SiO_4Cl_2:Eu^{2+},Mn^{2+}$,[18] $Ba_2Mg(PO_4)_2:Eu^{2+}$ [19] and $Sr_3(Al_2O_5)Cl_2:Eu^{2+}$.[20] To the best of our knowledge, the crystal structures and luminescence properties of $Na_3K(Si_{1-x}Al_x)_8O_{16\pm\delta}:Eu^{2+}$ have not yet been reported in the literature. The nepheline, $Na_3K(Si_{1-x}Al_x)_8O_{16\pm\delta}$, can be regarded as derived from that of tridymite by the replacement of one-half of the silicon ions by aluminium, and for charge balance alkali ions have to be incorporated into channels of the $(Al–Si)O_4$ tetrahedral framework. In tridymite the channels parallel with the hexagonal *c*-axis exhibit six-fold symmetry, whereas in nepheline only the channel in the origin retains the high symmetry. The adjacent ones, however, are distorted.[21,22] Thus the nepheline unit cell contains one wide channel of high symmetry where K ions are located and three kinds of distortions of channels which contain the smaller sodium ions. In this paper, we present an investigation of the luminescence of the yellow-emitting $Na_3K(Si_{1-x}Al_x)_8O_{16\pm\delta}:Eu^{2+}$ phosphor, where δ is oxygen nonstoichiometry varying from −0.4 to +0.24 depending

[a]*Department of Materials Science and Engineering, Korea Advanced Institute of Science and Technology, 291 Daehak-ro, Yuseong-gu, Daejeon, 305-701, Republic of Korea. E-mail: dyjeon@kaist.ac.kr*
[b]*School of Materials Science and Engineering, Chonnam National University, 300 Yongbong-Dong, Buk-Gu, Gwangju, 500-757, Republic of Korea*

on the x value. In addition, white-light n-UV LEDs possessing excellent CRI (R_a) values and warm correlated color temperatures were fabricated using a phosphor blend of blue-emitting $BaMgAl_{10}O_{17}:Eu^{2+}$ and yellow-emitting $Na_3K(Si_{1-x}Al_x)_8O_{16\pm\delta}:Eu^{2+}$ and their optical properties were investigated.

2 Experimental

2.1 Sample preparation

The powder samples of $Na_3K(Si_{1-x}Al_x)_8O_{16\pm\delta}:Eu^{2+}$ ($0.4 \leq x \leq 0.6$) were prepared by the solution method using proper amounts of aluminium nitrate nonahydrate ($Al(NO_3)_3\cdot 9H_2O \geq 98\%$, Aldrich), sodium nitrite ($NaNO_3 \geq 99.99\%$, Aldrich), potassium nitrate ($KNO_3 \geq 98\%$, Aldrich), tetraethyl orthosilicate (TEOS, 99.999%; Aldrich), and europium(III) chloride hexahydrate ($EuCl_3\cdot 6H_2O$, 99.99%; Aldrich) as starting materials. All materials were dissolved in water (solution A) except for TEOS, which was mixed with ethanol (solution B). After two types of solutions (A and B) were prepared, they were thoroughly mixed together. The mixtures were subsequently heated in an oven at 120 °C until the solvent dried up completely. The dried powders were then annealed at 1300 °C in a reducing atmosphere of H_2/N_2 (5%/95%) for 3 h.

2.2 Characterization

Room temperature photoluminescence (PL) spectra were recorded using an F-7000 Hitachi fluorescence spectrophotometer, PL System, equipped with a xenon lamp (500 W) as an excitation source scanning the wavelength of 400–800 nm. The X-ray diffraction (XRD, Philips X'Pert) data were obtained over a range of $20° \leq 2\theta \leq 120°$ at steps of 0.026° with Cu-Kα radiation. Crystal structure refinement employed the Rietveld method which is implemented in the General Structure Analysis System (GSAS) software suite.[23] For time-resolved PL measurements, a streak camera C4334 (Hamamashu, Japan) was used to excite the phosphor at a wavelength of 374 nm.

2.3 Fabrication of white-emitting LEDs

The white-emitting UV LED was fabricated using a mixture of silicon resin, yellow-emitting $Na_3K(Si_{0.52}Al_{0.48})_8O_{16.08}:Eu^{2+}$ phosphor and blue-emitting $BaMgAl_{10}O_{17}:Eu^{2+}$ ($BAM:Eu^{2+}$) phosphor, which were dropped onto a 395 nm UV chip.

Optical properties such as luminescence spectra, color-rendering index (R_a), color temperature (CCT) and Commission International de I'Eclairage (CIE) color coordinates of the white-emitting LEDs were characterized using a Xe lamp (500 W) with a DARSA PRO 5100 PL system (PSI Scientific Co. Ltd., Korea) and evaluated under forward biases of varying constant currents in which the light output was collected and measured using an integrating sphere.

3 Results and discussion

3.1 XRD refinement and crystal structure of $Na_3K(Si_{1-x}Al_x)_8O_{16\pm\delta}$

Fig. 1 shows the data (circles), fitted (red line), and difference (bottom) XRD profiles for the Rietveld refinement of the

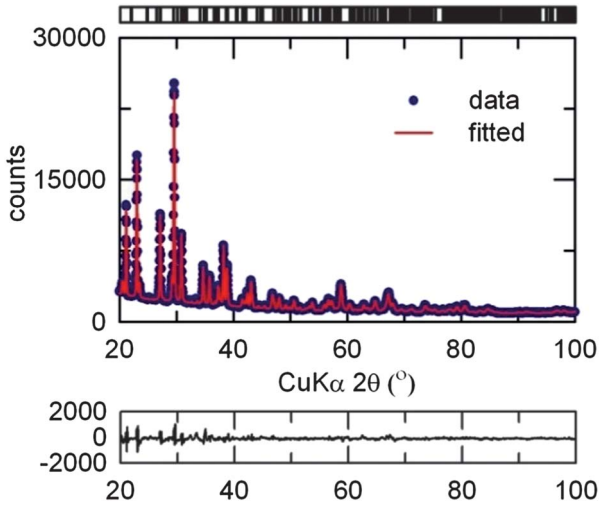

Fig. 1 Rietveld refinement of the powder XRD profile of $Na_3K(Si_{0.5}Al_{0.5})_8O_{16}:Eu^{2+}$. Data (circles), fitted (red line), and difference profiles are displayed along with expected reflection position.

$(Na_{0.95}Eu_{0.05})_3K(Si_{0.5}Al_{0.5})_8O_{16}$ phosphor. $(Na_{0.95}Eu_{0.05})_3K(Si_{0.5}Al_{0.5})_8O_{16}$ crystallized in a hexagonal unit cell with space group $P6_3$ and cell parameters $a = b = 10.052(2)$ Å, $c = 8.4075(7)$ Å, and cell volume = 849.52 Å^3. The refinement finally converged to $R_p = 4.95\%$, $R_{wp} = 3.02\%$ and $\chi^2 = 3.28$ is listed in Table 1. Structural parameters of the $(Na_{0.95}Eu_{0.05})_3K(Si_{0.5}Al_{0.5})_8O_{16}$ phosphor are shown in Table 2. Fig. 2a and b show a schematic of the $Na_3K(Si_{0.5}Al_{0.5})_8O_{16}$ crystal structure and the coordination environment of the Na atom, respectively. The substitution site of the Na^+ ion for the Eu^{2+} ion is one which has site symmetry 1. Structurally, nepheline can be described as a stuffed tridymite. This subset of the feldspathoid group consists of minerals with the same framework structure as SiO_2 tridymite; sixfold rings of SiO_4 tetrahedra join to form sheets, which stack in an ABAB sequence to give a framework. Charge balance is maintained by alkali cations—usually Na and K—which are located in the large cavities in the framework. The aluminosilicate framework collapses around these stuffing cations to minimize the coulombic energy. The majority of natural nephelines have a slight excess of Si over Al, balanced by vacancies on the K sites.[24]

Table 1 Rietveld refinement and crystal property data of $Na_3K(Si_{1-x}Al_x)_8O_{16\pm\delta}:Eu^{2+}$ phosphors. The numbers in parentheses are the estimated standard deviations of the last significant figure

Formula	$Na_3K(Si_{0.5}Al_{0.5})_8O_{16}$
Radiation type	CuKα
2θ range (degree)	20–100
T/K	295
Symmetry	Hexagonal
Space group	$P6_3$
a/Å	10.052(2)
c/Å	8.4075(7)
Z	2
R_p	4.95%
R_{wp}	3.02%
χ^2	3.28

Table 2 Refined structural parameters for $Na_3K(Si_{0.5}Al_{0.5})_8O_{16}$ obtained from Rietveld refinement using X-ray powder diffraction data at room temperature. The numbers in parentheses are the estimated standard deviations of the last significant figure

	x	y	z	g^a	$100\times\ U_{iso}/Å^{2b}$
Na	0.9951(6)	0.4446(4)	0.9986(1)	1.0	0.602(1)
K	0	0	0.0090(3)	1.0	4.177(2)
Al1	1/3	2/3	0.2045(1)	0.5	0.443(2)
Si1	1/3	2/3	0.2045(1)	0.5	0.443(2)
Al2	1/3	2/3	0.8205(1)	0.5	6.044(1)
Si2	1/3	2/3	0.8205(1)	0.5	6.044(1)
Al3	0.0928(1)	0.3286(2)	0.3156(2)	0.2	0.779(2)
Si3	0.0928(1)	0.3286(2)	0.3156(2)	0.8	0.779(2)
Al4	0.0996(1)	0.3465(1)	0.6951(1)	0.8	3.300(1)
Si4	0.0996(1)	0.3465(1)	0.6951(1)	0.2	3.300(1)
O1	0.301921	0.693610	0.9847(2)	0.333	0.333(1)
O2	0.0340(1)	0.3269(2)	0.5083(2)	1.0	6.217(2)
O3	0.1678(2)	0.5167(1)	0.7329(1)	1.0	0. 585(2)
O4	0.1702(1)	0.5112(1)	0.2378(2)	1.0	0.170(1)
O5	0.2235(1)	0.2837(1)	0.3112(1)	1.0	6.937(1)
O6	0.2225(2)	0.2589(1)	0.6923(1)	1.0	2.031(1)

[a] Constraint on occupancy: $g(Al1) + g(Si1) = g(Al2) + g(Si2) = g(Al3) + g(Si3) = g(Al4) + g(Si4) = 1.0$. [b] Constraint on isotropic thermal factor: $U_{iso}(Al1) = U_{iso}(Si1)$, $U_{iso}(Al2) = U_{iso}(Si2)$, $U_{iso}(Al3) = U_{iso}(Si3)$, $U_{iso}(Al4) = U_{iso}(Si4)$.

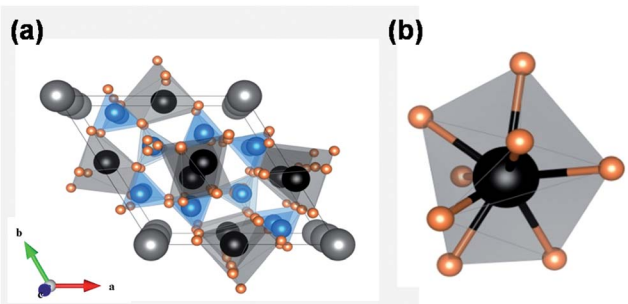

Fig. 2 (a) Unit-cell representation of $Na_3K(Si_{0.5}Al_{0.5})_8O_{16}$ and (b) coordination geometry of the EuO_8 polyhedron therein. Black, light gray, blue, and orange spheres represent Na, K, Al/Si, and O atoms, respectively. Blue spheres are shared by Al and Si atoms.

3.2 Photoluminescence of $Na_3K(Si_{1-x}Al_x)_8O_{16\pm\delta}$

Fig. 3 shows the PLE and PL spectra of the $Na_3K(Si_{1-x}Al_x)_8O_{16\pm\delta}:Eu^{2+}$ phosphor depending on the Al^{3+} content (x value) in the host lattice. By varying x value the non-stoichiometry (indicated as a $\pm\delta$) of oxygen ions varied and the non-stoichiometry of oxygen ions is expected to influence the luminescence properties of $Na_3K(Si_{1-x}Al_x)_8O_{16\pm\delta}:Eu^{2+}$ phosphors such as position luminescence spectrum and intensity. The PL emission intensity was enhanced and the central emission wavelength was red-shifted with changing x value. The emission intensity strongly depended on the stoichiometry of the $Na_3K(Si_{1-x}Al_x)_8O_{16.24}:Eu^{2+}$ phosphor. At $x = 0.48$ mol the δ value is almost ignored and the value is close to the stoichiometry of the $Na_3K(Si_{0.5}Al_{0.5})_8O_{16}:Eu^{2+}$ composition. The δ value strongly affected emission intensity. With increasing x value, the non-stoichiometry of oxygen ions became a $-\delta$ value and oxygen vacancies formed acting as luminescent killer sites and decreased emission intensity was observed with increasing x.

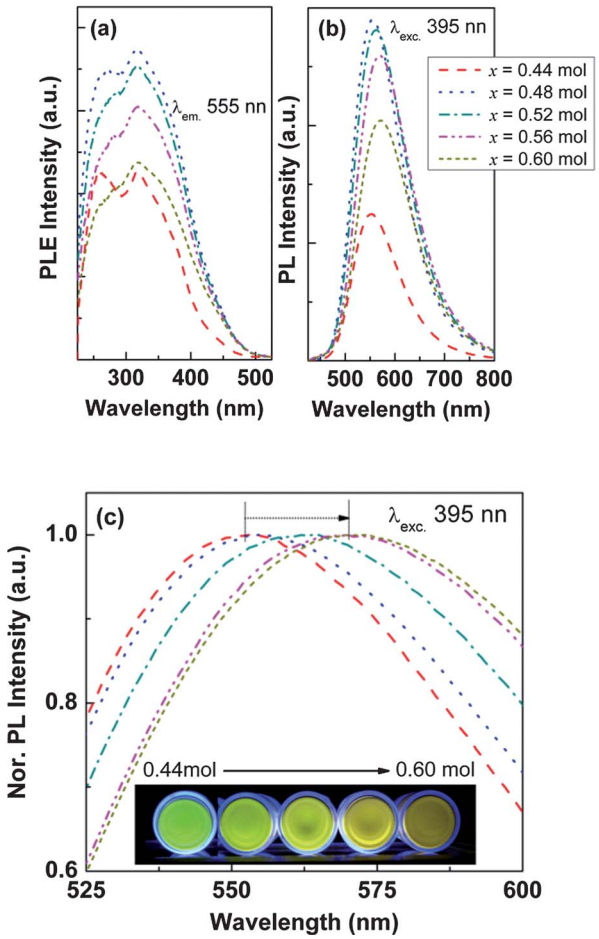

Fig. 3 Dependence (a) excitation, (b) emission, and (c) normalized emission spectra of the $Na_3K(Si_{1-x}Al_x)_8O_{16\pm\delta}:Eu^{2+}$ phosphor ($0.44 \leq x \leq 0.60$ mol) on concentration of Al^{3+}.

Such red-shift was attributed to the change of the surrounding environment of the Eu^{2+} ions due to the lattice distortion originated from oxygen vacancies. The $4f^7 \rightarrow 4f^65d$ transition of Eu^{2+} is strongly dependent on the host lattice because the outermost $5d$ orbit is very sensitive to its crystal-field surroundings. As with incorporation of Al^{3+} in Si^{4+} sites, it was the case that the tetrahedral symmetry around Eu^{2+} lowered. Due to the lowered symmetry, crystal field splitting of $5d$ band Eu^{2+} increased so that the emission band of Eu^{2+} shifts to a longer wavelength.[25]

When Si^{4+} sites were substituted with Al^{3+} ions, no phase change was observed up to 0.56 mol of Al^{3+} contents; however, at Al^{3+} contents higher than 0.60 mol, an impurity phase, $Na_{1.45}Al_{1.45}Si_{0.55}O_4$, was observed. Fig. 4 shows powder XRD patterns of the $Na_3K(Si_{1-x}Al_x)_8O_{16\pm\delta}:Eu^{2+}$ phosphor. As the amount of Al^{3+} ions was increased in the host lattice, the main diffraction peak of (202) shifted to lower diffraction angles from 29.60° for $Na_3K(Si_{0.56}Al_{0.44})_8O_{16.24}:Eu^{2+}$ to 29.40° for $Na_3K(Si_{0.40}Al_{0.60})_8O_{15.6}:Eu^{2+}$. This change of the XRD patterns indicates the distorted lattice by substitution of Si^{4+} with Al^{3+} ions. As a result, the emission band of $Na_3K(Si_{1-x}Al_x)_8O_{16\pm\delta}:Eu^{2+}$ was changed as shown in Fig. 2. The corresponding luminescence properties and calculated lattice parameters of $Na_3K(Si_{1-x}Al_x)_8O_{16\pm\delta}:Eu^{2+}$ phosphors are given in Table 3. In

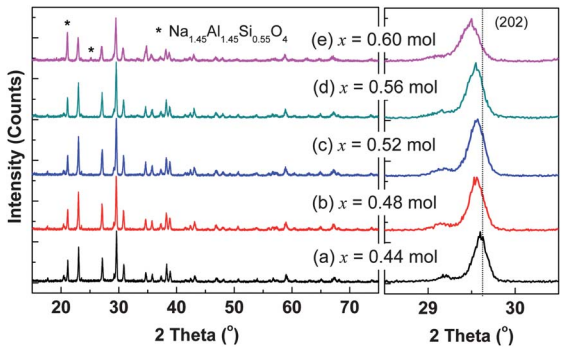

Fig. 4 Powder XRD patterns for $Na_3K(Si_{1-x}Al_x)_8O_{16\pm\delta}:Eu^{2+}$ phosphors with various x values.

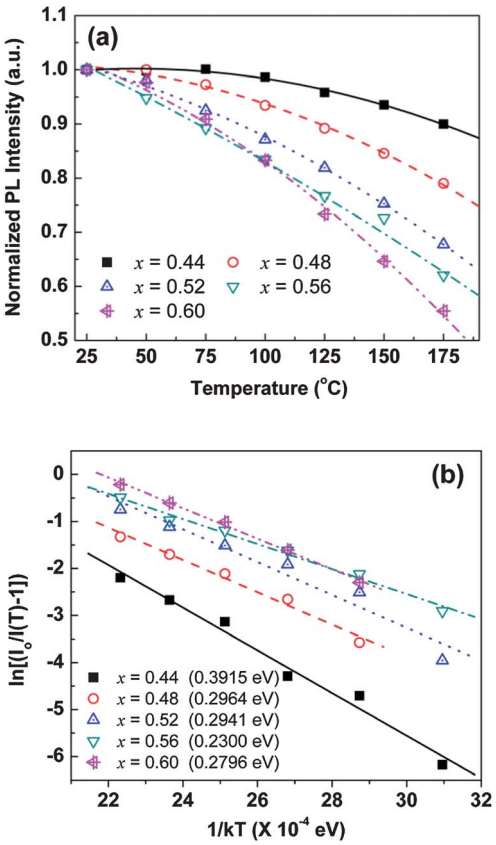

Fig. 5 (a) Temperature dependence of relative emission intensity and (b) the activation energy (ΔE) of $Na_3K(Si_{1-x}Al_x)_8O_{16\pm\delta}:Eu^{2+}$ phosphors under 395 nm excitation as a function of the Al^{3+} contents (x).

general, the temperature dependence of phosphors used in phosphor-converted W-LEDs is important because it exerts considerable influence on the light output and color-rendering index. For application in LEDs, the thermal stability of phosphors is one of the important issues to be addressed. Temperature dependence of relative emission intensities for $Na_3K(Si_{1-x}Al_x)_8O_{16\pm\delta}:Eu^{2+}$ as a function of Al^{3+} content (x) under 395 nm excitation is shown in Fig. 5. The relative emission intensity decreases with an increase in temperature and the thermal degradation of the $Na_3K(Si_{1-x}Al_x)_8O_{16\pm\delta}:Eu^{2+}$ phosphor becomes enhanced with increasing Al^{3+} contents (x). Observed were decays of 94%, 85%, 75% 73% and 65% at 150 °C depending on increase in Al^{3+} contents (x) for $Na_3K(Si_{1-x}Al_x)_8O_{16\pm\delta}:Eu^{2+}$, respectively. The thermal degradation of $Na_3K(Si_{1-x}Al_x)_8O_{16\pm\delta}:Eu^{2+}$ phosphors occurs due to the nonradiative transition from the excited state to the ground state. At low temperatures the radiative transition from nearly the bottom of the excited state to the ground state occurs and no temperature dependence is observed. However, when temperature increases, the excited state obtains thermal energy and cross-over to the ground state and as a result nonradiative transition becomes more dominant. The process enhances with increasing temperature and the luminescence intensity becomes weak at high temperatures. With the increase of the Al^{3+} ion content, the number of oxygen vacancies of the host lattice strongly increases, which destroys the lattice structure[26] due to the requirement of charge neutrality during substitution of Si^{4+} with the Al^{3+} ion. The oxygen vacancies behave as nonradiative recombination centers and the nonradiative defects are largely responsible for rapid thermal quenching of Eu^{2+} luminescence. Therefore, thermal activation energy (ΔE) is required to raise the electron from the relaxed excited level to the host lattice conduction band.[27] It can also be assumed that the thermal quenching as in eqn (1) originates from energy transfer to defect centers (killer centers) by a nonradiative recombination process. The thermal activation energies (ΔE) of $Na_3K(Si_{1-x}Al_x)_8O_{16\pm\delta}:Eu^{2+}$ phosphors were calculated by

$$I(T) = \frac{I_0}{1 + A\exp\left(\frac{-\Delta E}{kT}\right)} \quad (1)$$

where I_0 and $I(T)$ are the emission intensities at room temperature and testing temperature, respectively, A is a constant and k is the Boltzmann constant (8.617×10^{-5} eV K^{-1}). In Fig. 5b, the plot of ln [$I_0/I(T) - 1$] *vs.* 1/(kT) indicates a linear relation. The ΔE was obtained to be 0.3915 eV and 0.2300 eV for

Table 3 Emission bands, Stokes shift, normalized PL intensity as well as CIE coordinates and lattice parameters of $Na_3K(Si_{1-x}Al_x)_8O_{16\pm\delta}:Eu^{2+}$ phosphors

					Lattice parameter/Å	
x	$\lambda_{em.}$/nm	Stokes shift/cm^{-1}	Normalized PL intensity (%)	CIE (x, y)	a	c
0.44	553	13 167	43	(0.4188, 0.5408)	10.0343	8.3628
0.48	555	13 232	100	(0.4272, 0.5360)	10.0439	8.3885
0.52	564	13 520	97	(0.4427, 0.5227)	10.0904	8.3941
0.56	570	13 707	89	(0.4588, 0.5091)	10.1310	8.3969
0.60	573	13 798	70	(0.4609, 0.5057)	10.2105	8.3995

$Na_3K(Si_{0.56}Al_{0.44})_8O_{16.24}:Eu^{2+}$ (x = 0.44 mol) and $Na_3K(Si_{0.40}Al_{0.56})_8O_{15.76}:Eu^{2+}$ (x = 0.56 mol) phosphors, respectively. The probability of nonradiative transition *via* thermal activation strongly depends on temperatures. The probability of nonradiative transition per unit time (α) is expressed in the equation below:[28]

$$\alpha = s\exp\left(\frac{-\Delta E}{kT}\right) \quad (2)$$

where s is the frequency factor (s^{-1}), k is the Boltzmann constant, T is the temperature, and ΔE is the activation energy for a nonradiative transition. Because s, k and ΔE are constant, it is clear that lower activation energy leads to greater probability of nonradiative transition, thereby causing a decrease in the emission intensity of the phosphors depending on the x value. It turns out that the thermal stability of the $Na_3K(Si_{0.52}Al_{0.48})_8O_{16.08}:Eu^{2+}$ phosphor is comparable to that of the $Y_3Al_5O_{12}:Ce^{3+}$ phosphor reported in the literature.[29,30] The results demonstrated that the $Na_3K(Si_{1-x}Al_x)_8O_{16\pm\delta}:Eu^{2+}$ phosphor could be a promising candidate phosphor for LED application. As can be seen from Fig. 6a and b, PL intensities of the phosphor increased with increasing Eu^{2+} content up to 5 mol % while decreased PL intensity was observed at Eu^{2+} contents higher than 5 mol% due to a well-known concentration quenching. At critical concentration, the average shortest distance between activator ions is equal to the critical distance R_c, and the critical distance R_c is suggested by Blasse,[31]

$$R_c \approx 2\left(\frac{3V}{4\pi X_c N}\right)^{\frac{1}{3}} \quad (3)$$

where V is a volume of the unit cell, X_c is the critical concentration, and N is the number of cations in the unit cell. Taking the values of $V = 849.52$ Å^3, $X_c = 0.05$, and $N = 2$, the R_c turned out to be 25.32 Å. From the results, it was confirmed that the energy transfers between Eu^{2+} ions in the $Na_3K(Si_{1-x}Al_x)_8O_{16\pm\delta}:Eu^{2+}$ phosphor were mainly electric dipole–dipole interactions and the optimized concentration (0.05 mol) obtained in this study was accurate. In order to explain the concentration quenching in more detail, normalized decay curves for the $Na_{3-y}K(Si_{1-x}Al_x)_8O_{16\pm\delta}:{}_yEu^{2+}$ ($0.01 \le y \le 0.06$ mol) phosphor under laser excitation at 374 nm are presented. These decays were analyzed at the maximum of Eu^{2+} emission at 550 nm. The measured lifetime (τ) of Eu^{2+} $5d \rightarrow 4f$ emission at 550 nm decreases with increasing Eu^{2+} concentration (y). In particular, the lifetime of Eu^{2+} decreased from 1.56 μs to 1.46 μs when the doped Eu^{2+} concentration increased from 0.02 mol to 0.06 mol. The measured lifetime is related to the total relaxation rate by:[32,33]

$$\frac{1}{\tau} = \frac{1}{\tau_0} + A_{nr} + P_t \quad (4)$$

where τ_0 is the radiative lifetime, A_{nr} is the nonradiative rate due to multiphonon relaxation, and P_t is the energy transfer rate between Eu^{2+} ions.

With increasing Eu^{2+} concentration, both the energy transfer rate between Eu^{2+}–Eu^{2+} and the probability of energy transfer to luminescent killer sites (such as defects) increased. As a result, the lifetime shortened with increasing Eu^{2+} concentration. As the

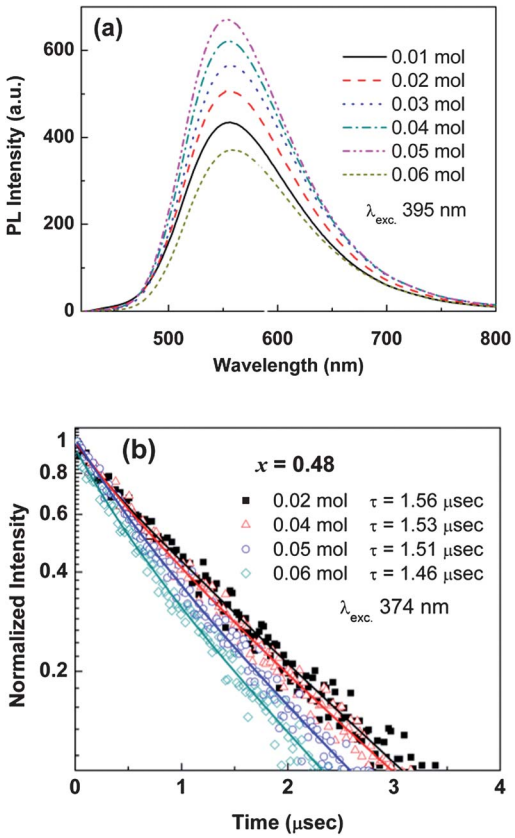

Fig. 6 Concentration dependence of relative emission intensity and decay curves of Eu^{2+} emission for $Na_3K(Si_{0.52}Al_{0.48})_8O_{16.08}:Eu^{2+}$ phosphors under 374 nm excitation, monitored at 550 nm.

Eu^{2+} concentration quenching results from energy transfer processes between Eu^{2+} ions, the observed decay investigation results also further support that concentration quenching occurs in the $Na_{3-y}K(Si_{1-x}Al_x)_8O_{16\pm\delta}:{}_yEu^{2+}$ ($0.01 \le y \le 0.06$ mol) phosphor.

3.3 Electroluminescence (EL) of $Na_3K(Si_{1-x}Al_x)_8O_{16\pm\delta}:Eu^{2+}$

In order to further investigate the potential of $Na_3K(Si_{1-x}Al_x)_8O_{16\pm\delta}:Eu^{2+}$ which has an internal quantum efficiency of ~51% in application of UV LED-pumped white-emitting LEDs, shown in Fig. 7 are the electroluminescent (EL) spectra and the CIE color coordinates (x, y), CCT and R_a of white-light UV LED with different driving currents. The EL spectra clearly show a near-UV band around 395 nm, a blue-emitting band corresponding to the $BaMgAl_{10}O_{17}:Eu^{2+}$ (BAM:Eu^{2+}) phosphor around 450 nm, and yellow-emitting bands corresponding to the $Na_3K(Si_{0.52}Al_{0.48})_8O_{16.08}:Eu^{2+}$ phosphors around 575 nm. Upon increasing the current from 10 mA to 50 mA, the EL intensity increased depending on the current. The deviation of CIE color coordinates was quite small. The Δx and Δy are calculated to be 0.0052 and 0.0098, respectively, as shown in Fig. 7b. The CIE color coordinates, correlated color temperature (CCT) and average color-rendering index R_a were (x, y) = (0.33, 0.29), 5952 K and 90, respectively. The full set of R_a and the average R_a are listed in Table 4.

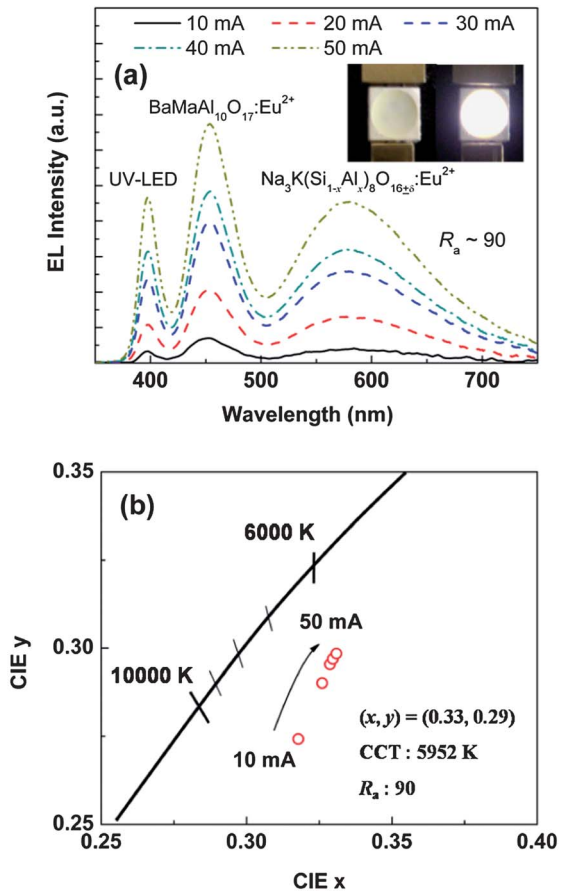

Fig. 7 (a) EL spectra and (b) the CIE color coordinates of blue-emitting BAM:Eu^{2+} and yellow-emitting $Na_3K(Si_{0.52}Al_{0.48})_8O_{16.08}:Eu^{2+}$ in conjunction with a near UV LED chip (λ_{ex} = 395 nm) with different driving currents; the insets show the photos of the LED package.

Table 4 Full set of 8 components of the CRI and the R_a of a 395 nm UV LED pumped with $Na_3K(Si_{0.52}Al_{0.48})_8O_{16.08}:Eu^{2+}$ + $BaMgAl_{10}O_{17}:Eu^{2+}$ (BAM:Eu^{2+}) phosphors

R_1	R_2	R_3	R_4	R_5	R_6	R_7	R_8	R_a
91	93	92	89	91	86	90	88	90

4 Conclusion

In this paper, a new yellow-emitting phosphor, $Na_3K(Si_{1-x}Al_x)_8O_{16\pm\delta}:Eu^{2+}$, which can be efficiently excited over a broad spectral range from 250 to 450 nm was synthesized by a wet chemical reaction method. We have successfully investigated their luminescence properties as a function of the Al^{3+} contents and it is found that the red-shifted PL emission wavelength depending on Al^{3+} content due to the splitting of the crystal field originated from crystal distortion. Moreover, the optimal doping concentration of Eu^{2+} was 0.05 mol and the critical distance was estimated to be 25.34 Å based upon the concentration quenching method. A warm white-emitting LED with CCT = 5952 K, R_a = 90, and CIE = (0.33, 0.29) was fabricated using a mixture of yellow-emitting $Na_3K(Si_{0.52}Al_{0.48})_8O_{16.08}:Eu^{2+}$ phosphor and blue-emitting $BaMgAl_{10}O_{17}:Eu^{2+}$ phosphor pumped by a 395 nm near-UV chip. These results indicate that the yellow-emitting $Na_3K(Si_{1-x}Al_x)_8O_{16\pm\delta}:Eu^{2+}$ phosphor can serve as a new promising candidate for application in white-emitting LEDs.

Notes and references

1 S. Nakamura, *Appl. Phys. Lett.*, 1993, **62**, 2390.
2 W. B. Im, Y. I. Kim, N. N. Fellows, H. Masui, G. A. Hirata, S. P. DenBaars and R. Seshadri, *Appl. Phys. Lett.*, 2008, **93**, 091905.
3 J. S. Kim, P. E. Jeon, J. C. Choi, H. L. Park, S. I. Mho and G. C. Kim, *Appl. Phys. Lett.*, 2004, **84**, 2931.
4 D. Haranath, H. Chander, P. Sharma and S. Singh, *Appl. Phys. Lett.*, 2006, **89**, 173118.
5 R. Kasuya, A. Kawano, T. Isobe, H. Kuma and J. Katano, *Appl. Phys. Lett.*, 2007, **91**, 111916.
6 H. Jang, Y. H. Won and D. Jeon, *Appl. Phys. B: Lasers Opt.*, 2009, **95**, 715.
7 Y. Chen, M. Gong, G. Wang and Q. Su, *Appl. Phys. Lett.*, 2007, **91**, 071117.
8 H. S. Jang, W. B. Im, D. C. Lee, D. Y. Jeon and S. S. Kim, *J. Lumin.*, 2007, **126**, 371.
9 M. Batentschuk, A. Osvet, G. Schierning, A. Klier, J. Schneider and A. Winnacker, *Radiat. Meas.*, 2004, **38**, 539.
10 J. K. Sheu, S. J. Chang, C. H. Kuo, Y. K. Su, L. W. Wu, Y. C. Lin, W. C. Lai, J. M. Tsai, G. C. Chi and R. K. Wu, *IEEE Photonics Technol. Lett.*, 2003, **15**, 18.
11 C.-H. Huang and T.-M. Chen, *Inorg. Chem.*, 2011, **50**, 5725.
12 G. Denis, P. Deniard, E. Gautron, F. Clabau, A. Garcia and S. Jobic, *Inorg. Chem.*, 2008, **47**, 4226.
13 M. Zhang, J. Wang, Q. Zhang, W. Ding and Q. Su, *Mater. Res. Bull.*, 2007, **42**, 33.
14 W. S. Song, Y. S. Kim and H. Yang, *Mater. Chem. Phys.*, 2009, **117**, 500.
15 Z. Yang, S. Wang, G. Yang, J. Tian, P. Li and X. Li, *Mater. Lett.*, 2007, **61**, 5258.
16 S. Levshov, I. Berezovskaya, N. Efryushina, B. Zadneprovskii and V. Dotsenko, *Inorg. Mater.*, 2011, **47**, 285.
17 X. Sun, J. Zhang, X. Zhang, Y. Luo and X. Wang, *J. Rare Earths*, 2008, **26**, 421.
18 W. J. Ding, J. Wang, Z. M. Liu, M. Zhang, Q. Su and J. K. Tang, *J. Electrochem. Soc.*, 2008, **155**, J122.
19 Z. C. Wu, M. L. Gong, J. X. Shi, G. Wang and Q. A. Su, *Chem. Lett.*, 2007, **36**, 410.
20 Y. Tang, *Appl. Phys. Lett.*, 2008, **93**, 131114.
21 B. Hippler and H. Böhm, *Z. Kristallogr.*, 1989, **187**, 39.
22 N. Foreman and D. R. Peacor, *Z. Kristallogr.*, 1970, **132**, 45.
23 A. C. Larson and R. B. V. Dreele, *Los Alamos National Laboratory Report LAUR*, 1994.
24 S. A. Hayward, A. K. A. Pryde, R. F. de Dombal, M. A. Carpenter and M. T. Dove, *Phys. Chem. Miner.*, 2000, **27**, 285.
25 J. K. Park, M. A. Lim, C. H. Kim, H. D. Park and S. Y. Choi, *Electrochem. Solid-State Lett.*, 2004, **7**, H23.
26 L. Sun, C. Qian, C. Liao, X. Wang and C. Yan, *Solid State Commun.*, 2001, **119**, 393.
27 A. M. Srivastava, H. A. Comanzo, S. Camardello, S. B. Chaney, M. Aycibin and U. Happek, *J. Lumin.*, 2009, **129**, 919.
28 X. Q. Piao, T. Horikawa, H. Hanzawa and K. Machida, *J. Electrochem. Soc.*, 2006, **153**, H232.
29 V. Bachmann, C. Ronda and A. Meijerink, *Chem. Mater.*, 2009, **21**, 2077.
30 X. Piao, K.-i. Machida, T. Horikawa, H. Hanzawa, Y. Shimomura and N. Kijima, *Chem. Mater.*, 2007, **19**, 4592.
31 G. Blasse, W. L. Wanmaker, J. W. Tervrugt and A. Bril, *Philips Res. Rep.*, 1968, **23**, 189.
32 D. Wang and N. Kodama, *J. Solid State Chem.*, 2009, **182**, 2219.
33 B. Henderson and G. F. Imbusch, *Optical Spectroscopy of Inorganic Solids*, Clarendon, Oxford, 1989, p. 151.

